

Accepted Manuscript

Title: Three-Dimensional Porous Metal-Nitrogen Doped Carbon Nanostructure as a Superior Non-Precious Electrocatalyst in Oxygen Reduction Reaction

Author: Seul Lee Young-Woo Lee Da-Hee Kwak Jin-Yeon Lee Sang-Beom Han Jung Inn Sohn Kyung-Won Park



PII: S1226-086X(16)30257-X
DOI: <http://dx.doi.org/doi:10.1016/j.jiec.2016.08.004>
Reference: JIEC 3039

To appear in:

Received date: 17-6-2016
Revised date: 3-8-2016
Accepted date: 3-8-2016

Please cite this article as: Seul Lee, Young-Woo Lee, Da-Hee Kwak, Jin-Yeon Lee, Sang-Beom Han, Jung Inn Sohn, Kyung-Won Park, Three-Dimensional Porous Metal-Nitrogen Doped Carbon Nanostructure as a Superior Non-Precious Electrocatalyst in Oxygen Reduction Reaction, Journal of Industrial and Engineering Chemistry <http://dx.doi.org/10.1016/j.jiec.2016.08.004>

This is a PDF file of an unedited manuscript that has been accepted for publication. As a service to our customers we are providing this early version of the manuscript. The manuscript will undergo copyediting, typesetting, and review of the resulting proof before it is published in its final form. Please note that during the production process errors may be discovered which could affect the content, and all legal disclaimers that apply to the journal pertain.

**Three-Dimensional Porous Metal-Nitrogen Doped Carbon
Nanostructure as a Superior Non-Precious Electrocatalyst in Oxygen
Reduction Reaction**

Seul Lee,^{a,1} Young-Woo Lee,^{a,b,1} Da-Hee Kwak,^a Jin-Yeon Lee,^a Sang-Beom Han,^a
Jung Inn Sohn,^b Kyung-Won Park^{a,*}

^a Department of Chemical Engineering, Soongsil University, Seoul 156-743, Republic of Korea.

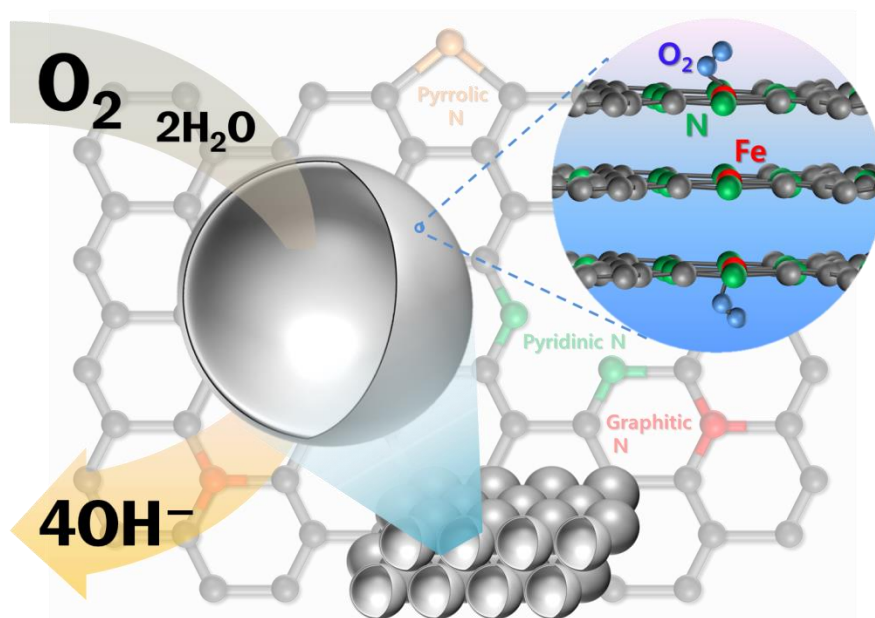
^b Department of Engineering Science, University of Oxford, Oxford OX1 3PJ, United Kingdom.

¹ These authors contributed equally to this work.

* Corresponding author. Tel: 82-2-820-0613. Fax: 82-2-812-5378.

E-mail address: kwpark@ssu.ac.kr (Prof. K.-W. Park).

Graphic Abstract



Research highlights

- Metal-nitrogen doped nanostructures were prepared using a one-pot synthesis.
- The nanostructures consisted of three-dimensionally hollow carbons.
- The nanostructures exhibited well-doped metal and nitrogen species.
- The nanostructures showed highly improved electrochemical properties in ORR.

Abstract

We report the porous transition metal-nitrogen doped carbon nanostructures as cathode catalysts using a well-stacked arrangement of template materials in the presence of polyvinylpyrrolidone as nitrogen and carbon sources and metal phthalocyanine as metal and nitrogen sources. The as-prepared nanostructures show high specific surface areas (105.73-228.13 m² g⁻¹), porous structure, and doped metal and nitrogen species (pyridinic-N, pyrrolic-N, and graphitic-N) into carbon structures. In particular, the porous Fe-N-doped carbon nanostructure exhibits excellent ORR electrocatalytic properties in alkaline electrolyte; i.e., electron transfer number close to 4, high half-wave potential (0.81 V), improved electrochemical stability (a slight decrease of ~31 mV in the half-wave potential after the stability test), and methanol tolerance.

Keywords: Porous carbon; Transition metal; Nitrogen; Electrocatalyst; Oxygen reduction reaction

1. Introduction

Polymer electrolyte membrane fuel cells (PEMFCs), operated by both reactions between hydrogen oxidation reaction (HOR) as an anodic reaction and oxygen reduction reaction (ORR) as a cathodic reaction, have been widely researched as one of the attractive energy power generation system owing to their many advantages such as high efficiency, low-temperature and stable operation, and environmental friendliness [1,2]. In spite of many efforts to develop and commercialize PEMFC system with high electrochemical performance, there still remain challenges, *i.e.*, use of precious electrocatalyst, long-term electrochemical stability, and low ORR efficiency. In particular, even though platinum (Pt) electrocatalyst has critical drawbacks with a high cost, kinetic limitation for oxygen diffusion rate, and stability deterioration in ORR, it has been mostly used as an attractive cathodic electrocatalyst for ORR in PEMFCs to date due to their remarkably excellent electrocatalytic activity [3,4]. In this regard, many scientific efforts have been recently focused on development of non-precious cathode electrocatalysts such as transition-metal complexes (*i.e.*, carbides, nitrides, and sulfides) and doped carbon nanomaterials (*i.e.*, nitrogen- and/or sulfur-doped carbon nanomaterials with graphene, nanotube, and nanofiber, and transition metal–N₄ chelate macrocycles) [5-16].

Among the non-precious cathodic electrocatalysts, transition metal and nitrogen doped carbon nanostructures (M-N-C, M = Fe and/or Co) have been intensively investigated as a potentially alternative non-precious electrocatalyst for Pt-based electrocatalyst replacement [17-19]. In the M-N-C nanostructures, doping sites, which are incorporated by the transition metals and/or nitrogen into the carbon-based nanostructures, can act as most efficient and electrochemically active sites for ORR.

Recently, the M-N-C electrocatalysts have been designed and developed to enhance electrochemical properties for ORR including electrochemical activity and stability as well as methanol-tolerance in comparison with those of Pt-based electrocatalysts [20-22]. Moreover, the active sites are directly correlated with large specific surface areas of the doped carbon nanostructures. To obtain nanostructures with high specific surface areas, many researches have great attention on developing porous and hollow, 3-dimensional nanostructures synthesized by polymer-assisted, nickel foam-derived and silica templating methods, and hydro-gel (or sol-gel) method [23-27]. In particular, among the various synthesis approaches, the porous nanostructures of M-N-C electrocatalysts with high specific surface areas have been intensively studied through spherical silica and polymer template methods [28-30].

Herein, we synthesized the porous metal-nitrogen doped carbon nanostructures (denoted as M-PVP-C, M = Fe or Co) for enhanced electrochemical properties in ORR using a well-stacked arrangement method with spherical silica beads in the presence of polyvinylpyrrolidone (PVP) as a carbon source and metal phthalocyanine (M-Pc) as nitrogen and metal sources. As illustrated in Fig. 1, to obtain the M-PVP-C, we used a multi-step process as follows: first step (Fig.1(a)) involves the laminated molding of SiO₂ beads as a well-stacked template in mixed solution with PVP, M-Pc, and DMF as a solvent; second step (Fig. 1(b)) is evaporation of the solvent at 60 °C; third step (Fig. 1(c)) is the carbonization of the mixed PVP and M-Pc coated on the SiO₂ beads at 900 °C; and final step (Fig. 1(d)) is to remove the SiO₂ template through HF washing process. Furthermore, the as-obtained M-PVP-C nanostructures present the well-designed porous structures with high specific surface areas as well as the transition metal and nitrogen atoms homogeneously doped into carbon nanostructures, and thus

exhibit the superior ORR activity, the methanol tolerance, and the excellent electrochemical stability comparable to those of commercial Pt electrocatalysts.

2. Experimental

2.1. Synthesis of the porous metal-nitrogen doped carbon nanostructures

For synthesis of the porous Fe or Co-nitrogen doped carbon nanostructures (denoted as M-PVP-C, M = Fe or Co), the 0.2 g cobalt(II) phthalocyanine (CoPc, Aldrich) or 0.2 g iron(II) phthalocyanine (FePc, Aldrich) as metal and nitrogen sources, and 0.8 g PVP (Aldrich, $M_w \sim 29,000$) as a main carbon source were mixed with 0.8 g silica beads (500 nm, Alfa Aesar) as a template and 20 mL dimethylformamide (DMF, Aldrich) in a 30 mL vial. The solutions were continuously stirred and then transferred in a glass dish to achieve a well-stacked structure. The as-prepared solutions were evaporated in an oven at 60 °C to completely remove DMF as a solvent. After complete drying, the evaporated powders were pyrolyzed under a nitrogen atmosphere at 900 °C for 3 h. The products were stirred in 10 vol% hydrofluoric acid solution for 1 h to completely remove the silica beads as a template and then washed with water and ethanol several times to remove the acid solution and impurities. The resulting samples were dried in an oven at 80 °C for 24 h. In addition, for comparison of the effect of transition metal doping, a porous nitrogen doped carbon nanostructure (denoted as PVP-C) was prepared in the absence of metal Pc.

2.2 Structural analysis

The as-prepared samples were characterized by FE-TEM and EDX analysis using a Philips Tecnai F20 system operating at 200 kV. The TEM samples were prepared by

placing a drop of the powder suspension in ethanol on a carbon-coated copper grid. FE-SEM images were obtained using a Carl Zeiss SIGMA microscope operating at 5 kV. Structural analysis of the carbon nanostructures was carried out using XRD method with a Bruker, D2 Phase System equipped with a Cu K α radiation source of $\lambda = 0.15406$ nm with a Ni filter. The tube current was 10 mA with a tube voltage of 30 kV. The 2θ between 20° and 80° was explored at a scan rate of 5° min⁻¹. Raman spectra were recorded on a High Resolution Micro Raman spectrometer (Horiba Jobin Yvon, LabRAM HR UV/Vis/NIR PL). XPS analysis was carried out with the Al K α X-ray source of 1486.8 eV at the chamber vacuum pressure of below 7.8 X 10⁻⁹ Torr and beam power of 200 W (Thermo Scientific, K-Alpha). All high resolution spectra were collected using the pass energy of 50 eV and a step size of 0.1 eV. Both ends of the baseline were set sufficiently far apart in order to avoid distorting the shape of the spectra, including the tails. A small variation of the range of the base line did not affect the relative number of fitted species (less than 1%). A nonlinear least-squares curve-fitting program was employed with a Gaussian–Lorentzian production function. The surface area and porosity of the as-synthesized samples were analyzed from nitrogen sorption measurement (Micromeritics ASAP 2020 adsorption analyzer).

2.3 Electrochemical analysis

The electrochemical properties of the catalysts were measured in a three-electrode cell at 25 °C using a potentiostat (PGSTAT302N, AUTOLAB). Pt wire and Hg/HgO (in saturated NaOH) were used as counter and reference electrodes, respectively. The catalyst inks were prepared by ultrasonically dispersing the catalyst powders in an appropriate amount of Millipore water and isopropanol. 0.5 μ L catalyst ink was dropped

onto the rotating disk electrode (0.0706 cm^2). After drying in an oven at 50°C , the total loading of each catalyst was $400 \mu\text{g cm}^{-2}$. To compare the electrochemical properties and the ORR activity of the catalysts, cyclic voltammograms (CVs) and linear sweep voltammograms (LSVs) were obtained in a 0.1 M NaOH solution. The transferred electron number (n) of the electrocatalysts in the ORR was determined using Koutecky-Levich plots.

The stability test for the ORR was carried out by applying between -0.4 and $+0.1 \text{ V}$ (vs. Hg/HgO) for 5000 cycles with a scan rate of 50 mV s^{-1} in an O_2 -saturated 0.1 M NaOH solution. Oxygen reduction current-potential curves before and after the stability test for the as-prepared electrocatalysts were obtained by linear sweep voltammetry at a rotation disk speed of 1600 rpm . The methanol-tolerance ORR activity of the electrocatalysts was evaluated in O_2 -saturated 0.1 M NaOH containing $0.5 \text{ M CH}_3\text{OH}$. To determine the role of iron/cobalt as the ORR active sites in the electrocatalysts, the ORR polarization curves for the samples were obtained in O_2 -saturated 0.1 M NaOH with 10 mM KCN . All potentials were calibrated with respect to the reversible hydrogen electrode (RHE) via the Nernst equation:

$$E_{\text{RHE}} = E_{\text{Hg/HgO}} + E_{\text{Hg/HgO}}^\circ + 0.059 * \text{pH}$$

$$E_{\text{RHE}} = E_{\text{Hg/HgO}} + 0.9 \text{ V}$$

where E_{RHE} is the potential of reversible hydrogen electrode, $E_{\text{Hg/HgO}}$ is the experimental potential through Hg/HgO , and $E_{\text{Hg/HgO}}^\circ$ is the standard potential of Hg/HgO (1.0 M saturated NaOH , 0.140 V). The electrochemical measurements were carried out in 0.1 M NaOH ($\text{pH}=13$).

3. Results and discussion

Figs. 2(a-c) and Figs. S1(a and b) show FE-SEM images of the as-prepared samples (PVP-C, Co-PVP-C, and Fe-PVP-C) synthesized using a template process. Figs. 2(d-f) show FE-TEM images of the nanostructures prepared using a template method. All of the nanostructures exhibited a porous spherical shape (~500 nm in diameter) with a thin wall of ~7 nm thickness, implying the complete transfer of SiO₂ beads as templates into the nanostructures accompanied by homogeneous coating on SiO₂ surfaces during the synthesis process. Furthermore, to identify the elemental distribution of the nanostructures, as shown in Figs. 2(g-i) and Figs. S1(c-f), the mapping images of carbon, nitrogen, and metals were obtained using TEM and SEM-EDX spectroscopy. It is evident that the as-prepared nanostructures contain carbon and nitrogen distributed along the walls of the porous nanostructures. In particular, despite the acid treatment during the synthesis, metal elements such as Co and Fe were incorporated with carbon and nitrogen species in the nanostructures, indicating that the presence of M-N bonding can play an essential role as active sites for the ORR.

In addition, the wide angle XRD patterns of the nanostructures are shown in Fig. S2. PVP-C shows broad diffraction peaks corresponding to (002) and (101) planes, indicating a low crystallinity of the carbon formed during the process. On the other hand, the peaks for (002) and (101) of Co-PVP-C and Fe-PVP-C suggest that the porous carbon nanostructures consist of a graphitic carbon framework, leading to a d-spacing of 0.34 nm, which is close to the d-spacing of graphite. As shown in the Raman spectra of the porous carbon nanostructures (Fig. S3), the two peaks are attributed to a G band at 1584 cm⁻¹ and D band at 1350 cm⁻¹, respectively. The G band is related to the E_{2g}

vibration mode of sp^2 carbon structures. The D band is related to the structural defects and partially disordered structures on the graphitic plane, which are caused by heteroatom (nitrogen or oxygen) doping [31,32]. The intensity ratio (I_D/I_G) of PVP-C, Co-PVP-C, and Fe-PVP-C exhibited a value of over 1. The higher I_D is believed to be attributed to the structural defects caused by pyrolyzed with PVP, CoPc, and FePc as nitrogen and/or metal dopants. To characterize the specific surface area and pore structure of the as-prepared nanostructures, nitrogen gas adsorption-desorption isotherms were obtained as shown in Fig. S4. The specific surface areas of PVP-C, Co-PVP-C, and Fe-PVP-C were 105.73, 120.78, and 228.13 $m^2 g^{-1}$, respectively. Recently, as similar reference material for this phenomenon, Du *et al.* reported the nitrogen-doped M/C (M = Fe, Co, Ni) porous nanocomposites with difference BET areas (100-200 $m^2 g^{-1}$) synthesized under same experimental condition, because a higher surface area of the nitrogen-doped M/C might be affected by the nature of precursor and the presence of transition metal [33]. Thus, in particular, the M-PVP-C nanostructures can be expected to exhibit a high ORR activity due to high surface area, which is directly associated with the active sites.

The chemical states of nitrogen for the as-prepared PVP-C, Co-PVP-C, and Fe-PVP-C were confirmed using XPS analysis. As indicated in Figs. 3(a-c), the high-resolution N 1s spectra of the as-prepared nanostructures were fitted with several different signals with binding energies of 398.2-398.7, 400.1-400.3, and 401.2-401.5 eV corresponding to pyridinic-N, pyrrolic-N, and graphitic-N states, respectively [34,35]. Among the nitrogen species, the existence of the pyrrolic-N states can be attributed to metal doping in the N-doped carbon nanostructure, forming metal-N₄ or metal-N₃ macrocycles with the pyrrolic-N and pyridinic-N bonding [36]. In particular, the charge

polarization and porous nanostructure can induce adsorption and reduction of oxygen molecules on the carbon atom surfaces to H_2O through a four electron reduction process [37]. Thus, the higher content of metal and pyrrolic-N along with the porous structure of Fe-PVP-C is responsible for an improved catalytic activity towards ORR in Fig. 3(d). Fig. S5(a) shows the $\text{Co}2\text{p}$ XPS spectra where the $\text{Co}2\text{p}_{3/2}$ and $\text{Co}2\text{p}_{1/2}$ components are distinguished along with two satellite peaks. The $\text{Co}2\text{p}_{3/2}$ and $\text{Co}2\text{p}_{1/2}$ peaks, located at binding energies of 781.6 and 796.8 eV, respectively, are the typical characteristics of the Co^{2+} species [38]. In Fig. S5(b), the $\text{Fe}2\text{p}_{3/2}$ spectrum of Fe-PVP-C consists of metallic and oxidation states of iron with binding energies of 707.5, 709.4 and 710.9 eV, corresponding to Fe, Fe^{2+} , and Fe^{3+} , respectively [39,40]. Furthermore, the content ratio of each element of the as-prepared nanostructures estimated by XPS analysis is summarized in Table 1.

To characterize the electrochemical properties for ORR, CVs of the as-prepared nanostructures were obtained in O_2 -saturated 0.1 M NaOH solution and compared with Pt/C (E-TEK Co.). The oxygen reduction peak potentials of PVP-C, Co-PVP-C, and Fe-PVP-C electrocatalysts in O_2 -saturated 0.1 M NaOH were 0.742, 0.748, and 0.753 V, respectively, implying that Fe-PVP-C showed an improved ORR activity in comparison with PVP-C and Co-PVP-C (Figs. 4(a-c)). The ORR activity of the as-prepared electrocatalysts was measured using LSV in O_2 -saturated 0.1 M NaOH. As shown in Fig. 4(d), the maximum current density of Fe-PVP-C is much greater than that of PVP-C and Co-PVP-C. Also, the Fe-PVP-C exhibited improved half-wave potential and current density at 0.7 V (0.81 V and 4.64 mA cm^{-2} , respectively) compared to PVP-C (0.74 V and 1.49 mA cm^{-2} , respectively) and Co-PVP-C (0.77 V and 3.41 mA cm^{-2} , respectively), as exhibited in Fig. 4(e). The higher current density of Fe-PVP-C at 0.7 V

is ascribed to the significantly more active sites on the high surface area of the porous nanostructure. The electron transfer number (n) of the electrocatalysts was calculated using Koutecky-Levich plots (Fig. 4(f)) and the following equations:

$$\frac{1}{j} = \frac{1}{j_L} + \frac{1}{j_K} = \frac{1}{B\omega^{1/2}} + \frac{1}{j_K} \quad (1)$$

$$B = 0.62nFC_O(D_O)^{2/3}\nu^{-1/6} \quad (2)$$

where j is the measured current density, j_K and j_L are the kinetic and diffusion limiting current density, respectively, F is the Faraday constant, D_O is the diffusion coefficient of O_2 , C_O is the bulk concentration of O_2 , ν is the kinetic viscosity of electrolyte, and ω is the angular velocity of the disk. The n values for the Fe-PVP-C toward ORR were determined to be approximately 4.0, indicating a complete oxygen reduction process in an alkaline solution. In contrast, the PVP-C exhibited a lower value of 2.2 as a deficient reduction reaction at 0.7 V. In recent, Masa *et al.* reported that the catalysts with relatively slow process rate in alkaline electrolyte may exhibit a $2e^-$ electron transfer process via intermediate of HO_2^- , as following reactions: (1) $O_2 + H_2O + 2e^- \rightarrow HO_2^- + OH^-$ at 0.3-0.7 V vs. RHE and (2) $HO_2^- + H_2O + 2e^- \rightarrow 3OH^-$ at < 0.3 V vs. RHE [41]. Due to the above process, the LSV curve of PVP-C exhibited a stepwise plateau region between 0.3 and 0.6 V, corresponding to a two-step sequential electrochemical process in ORR. Furthermore, Table S1 shows comparison of the electrocatalytic properties of previously reported other non-precious electrocatalysts for ORR. In the present study, the Fe-PVP-C shows remarkably enhanced ORR electrocatalytic activity *i.e.*, the higher half-wave potential and electron transfer number close to 4, compared to the non-precious electrocatalysts reported in other groups. To evaluate the electrochemical stability of the electrocatalysts for the ORR, a test was

carried out by applying linear potential sweeps between 0.6 and 1.0 V for 5000 cycles with a scan rate of 50 mV s^{-1} in O_2 -saturated 0.1 M NaOH. Fig. S6 shows the LSV curves of Fe-PVP-C for the ORR before and after the stability test compared to Pt/C. In the case of half-wave potentials, Fe-PVP-C exhibited a slight decrease of $\sim 31 \text{ mV}$ after the stability test, representing an improved stability of Fe-PVP-C electrocatalyst towards the ORR, in comparison with Pt/C ($\sim 65 \text{ mV}$).

Furthermore, in direct methanol fuel cells (DMFCs), a crossover of methanol as a fuel at the anode to a cathode is a critical problem, resulting in deteriorated cell performance due to reduced fuel efficiency in the anode and mixed potential in the cathode [42]. Thus, the methanol tolerance of cathode catalysts for the ORR in DMFCs should be required. To characterize the methanol-tolerance of the electrocatalysts during the ORR, LSVs were obtained in O_2 -saturated 0.1 M NaOH with and without 0.5 M CH_3OH (Fig. 5). The porous nanostructure electrocatalysts maintained the ORR activity regardless of the presence of CH_3OH in the oxygen reduction process, whereas Pt/C showed seriously decreased activity for the ORR in the electrolyte containing CH_3OH . This means that the porous carbon nanostructures as ORR electrocatalysts have an excellent methanol-tolerance, which can prevent the reduced cell potential caused by the mixed potential.

To determine the role of iron/cobalt as active catalytic sites for ORR in M-PVP-C as an electrocatalyst, the ORR activity was compared in O_2 -saturated 0.1 M NaOH with and without 10 mM KCN (Fig. S7). In general, it has been known that CN^- ions can coordinate with iron/cobalt, thus resulting in poisoning iron/cobalt active sites toward ORR. Co-PVP-C and Fe-PVP-C exhibited seriously deteriorated ORR activity; *i.e.*, increased negative shift of the ORR potential and decreased diffusion-limiting current,

resulting from the diminished catalytic active sites due to blocking of the iron sites by CN^- ions [43,44]. This suggests that both the transition consisted of in the M-PVP-C are crucial active sites for ORR catalytic activity. In contrast, PVP-C with nitrogen functionalities as a sole active site showed less ORR activity loss in O_2 -saturated 0.1 M NaOH with and without CN^- . As a result, improved electrochemical properties of the M-PVP-C electrocatalysts for the ORR may be attributed to the main portion of active sites such as Fe/Co-N and pyrrolic-N, and the high specific surface areas of the porous nanostructures. However, to elaborately characterize the actual ORR performance of the M-PVP-C electrocatalysts, further works will be carried out using an actual system for alkaline fuel cells.

4. Conclusions

We prepared porous metal-nitrogen doped carbon nanostructures as a cathode catalyst for ORR using a one-pot process in the presence of metal Pc as metal, carbon, and nitrogen sources. The as-prepared doped carbon nanostructures exhibited high specific surface area, well-defined porous structures, and homogeneous metal and nitrogen doping into a carbon structure. Especially, FePc and CoPc-derived carbon as a cathode catalyst having large specific surface area and high doping contents of metal and nitrogen species showed the high-performance ORR in an alkaline medium, i.e. improved half-wave potential, high kinetic current density, complete electron-transfer number, excellent electrochemical stability, and methanol-tolerance.

Acknowledgments

This work was supported by the Energy Technology R&D Program of the Korea Institute of Energy Technology Evaluation and Planning (KETEP), granted financial resource from the Ministry of Trade, Industry & Energy, Republic of Korea. (No. 20138520030800 and No. 20153030031670).

References

- [1] W. Vielstich, A. Lamm, H. Gasteiger, Handbook of Fuel Cells: Fundamentals, Technology and Applications, Wiley, United Kingdom, 2009.
- [2] S. M. M. Ehteshami, A. Taheri, S. H. Chan. Adroher, J. Ind. Eng. Chem. 34 (2016) 1-8.
- [3] Y.-W. Lee, S. N. Cha, K.-W. Park, J. I. Sohn, J. M. Kim, J. Nanomater. 2015 (2015) 273720. DOI: 10.1155/2015/273720.
- [4] W. Sheng, H. A. Gastelger, Y. Shao-Horn, J. Electrochem. Soc. 157 (2010) B1529-B1536.
- [5] A.-R. Ko, Y.-W. Lee, J.-S. Moon, S.-B. Han, G. Cao, K.-W. Park, Appl. Catal. A-Gen. 477 (2014) 102-108.
- [6] T. Odedairo, X. Yan, J. Ma, Y. Jiao, X. Yao, A. Du, Z. Zhu, ACS Appl. Mater. Interfaces 7 (2015) 21373-21380.
- [7] K. C. Heo, K. S. Nahm, S.-H. Lee, P. Kim, L. J. Ind. Eng. Chem. 17 (2011) 304-309.
- [8] C. W. B. Bezerra, L. Zhang, K. Lee, H. Liu, A. L. B. Marques, E. P. Marques, H. Wang, J. Zhang, Electrochim. Acta 53 (2008) 4937-4951.
- [9] P. Chen, T.-Y. Xiao, Y.-H. Qian, S.-S. Li, S.-H. Yu, Adv. Mater. 25 (2013) 3192-3196.
- [10] L. Qu, Y. Liu, J.-B. Baek, L. Dai, ACS Nano 3 (2010) 1321-1326.
- [11] K. Gong, F. Du, Z. Xia, M. Durstock, L. Dai, Science 323 (2009) 760-764.
- [12] Y. Li, W. Zhou, H. Wang, L. Xie, Y. Liang, F. Wei, J.-C. Idrobo, S. J. Pennycook, H. Dai, Nat. Nanotechnol. 7 (2012) 394-400.

- [13] R. Liu, C. Malotki, L. Arnold, N. Koshino, H. Higashimura, M. Baumgarten, K. Müllen, *J. Am. Chem. Soc.* 133 (2011) 10372-10375.
- [14] H. Tang, H. Yin, J. Wang, N. Yang, D. Wang, Z. Tang, *Angew. Chem. Int. Ed.* 52 (2013) 5585-5589.
- [15] H.-X. Zhong, J. Wang, Y.-W. Zhang, W.-L. Xu, W. Xing, D. Xu, Y.-F. Zhang, X.-B. Zhang, *Angew. Chem. Int. Ed.* 53 (2014) 14235-14239.
- [16] J. Wang, K. Li, H.-X. Zhong, D. Xu, Z.-L. Wang, Z. Jiang, Z.-J. Wu, X.-B. Zhang, *Angew. Chem. Int. Ed.* 54 (2015) 10530-10534.
- [17] M. Lan, G. Fan, Q. Chen, F. Li, *J. Ind. Eng. Chem.* 20 (2014) 1523-1531.
- [18] J. Y. Cheon, T. Kim, Y. M. Choi, H. Y. Jeong, M. G. Kim, Y. J. Sa, J. Kim, Z. Lee, T.-H. Yang, K. Kwon, O. Terasaki, G.-G. Park, R. R. Adzic, S. H. Joo, *Sci. Rep.* 3 (2013) 2715-2722.
- [19] J. Masa, W. Xia, M. Muhler, W. Schuhmann, *Angew. Chem. Int. Ed.* 54 (2015) 10102-10120.
- [20] H. Peng, Z. Mo, S. Liao, H. Liang, L. Yang, F. Luo, H. Song, Y. Zhong, B. Zhang, *Sci. Rep.* 3 (2013) 1765-1771.
- [21] Y.-W. Lee, G.-H. An, S. Lee, J. Hong, B.-S. Kim, J. Lee, D.-H. Kwak, H.-J. Ahn, W. Huh, S. N. Cha, K.-W. Park, J. I. Sohn, J. M. Kim, *Catal. Sci. Technol.* 6 (2016) 2085-2091.
- [22] S. Zhang, H. Zhang, Q. Liu, S. Chen, *J. Mater. Chem. A* 1 (2013) 3302-3308.
- [23] S. Zhang, S. Chen, *Catalysts* 5 (2015) 1202-1210.
- [24] J. Wang, H.-X. Zhong, Y.-L. Qin, X.-B. Zhang, *Angew. Chem. Int. Ed.* 52 (2013) 5248-5253.

- [25] J. Xu, Y. Zhao, C. Shen, L. Guan, *ACS Appl. Mater. Interfaces* 5 (2013) 12594-12601.
- [26] W. Zhou, K. Zhou, D. Hou, X. Liu, G. Li, Y. Sang, H. Liu, L. Li, S. Chen, *ACS Appl. Mater. Interfaces* 6 (2014) 21534-21540.
- [27] Z.-L.Wang, D. Xu, H.-X. Zhong, J. Wang, F.-L. Meng, X.-B. Zhang, *Gelatin- Sci. Adv.* 1 (2015) e1400035.
- [28] J. Liang, Y. Zheng, J. Chen, J. Liu, D. Hulicova-Jurcakova, M. Jaroniec, S. Z. Qiao, *Angew. Chem. Int. Ed.* 51 (2012) 3892-3896.
- [29] E. Antolini, *Appl. Catal. B-Environ.* 88 (2009) 1-24.
- [30] H. Chang, S. H. Joo, C. Pak, *J. Mater. Chem.* 17 (2007) 3078-3088.
- [31] M. S. Dresselhaus, G. Dresselhaus, R. Saito, A. Jorio, *Phys. Rep.* 409 (2005) 47-99.
- [32] Y. Shao, S. Zhang, M. H. Engelhard, G. Li, G. Shao, Y. Wang, J. Liu, I. A. Aksay, Y. Lin, *J. Mater. Chem.* 20 (2010) 7491-7496.
- [33] J. Du, F. Cheng, S. Wang, T. Zhang, J. Chen, *Sci. Rep.* 4 (2014) 4386.
- [34] H. Wang, T. Maiyalagan, X. Wang, *ACS Catal.* 2 (2012) 781-794.
- [35] C. Zhang, R. Hao, H. Liao, Y. Hou, *Nano Energy* 2 (2013) 88-97.
- [36] K. M. Kadish, K. M. Smith, R. Guillard, *Handbook of Porphyrin Science with Applications to Chemistry, Physics Materials Science, Engineering, Biology and Medicine*, World Scientific, Singapore, 2012.
- [37] L. Zhang, Z. Xia, *J. Phys. Chem. C* 115 (2011) 11170-11176.
- [38] Q. He, Q. Li, S. Khene, X. Ren, F. E. López-Suárez, D. Lozano-Castelló, A. Bueno-López, G. Wu, *J. Phys. Chem. C* 117 (2013) 8697-8707.

- [39] J. F. Moulder, W. F. Stickle, P. E. Sobol, K. D. Bomben, Handbook of X-ray Photoelectron Spectroscopy, Physical Electronics, Inc., United State of America, 1995.
- [40] S. Pylypenko, S. Mukherjee, T. S. Olson, P. Atanassov, *Electrochim. Acta* 53 (2008) 7875-7883.
- [41] J. Masa, A. Zhao, W. Xia, M. Muhler, W. Schuhmann, *Electrochim. Acta* 128 (2014) 271-278.
- [42] H. Liu, J. Zhang, *Electrocatalysis of Direct Methanol Fuel Cells*, WILEY-VCH: Federal Republic of Germany, 2009.
- [43] S. Gupta, C. Fierro, E. Yeager, *J. Electroanal. Chem.* 306 (1991) 239-250.
- [44] M. S. Thorum, J. M. Hankett, A. A. Gewirth, *J. Phys. Chem. Lett.* 2 (2011) 295-298.

Figure captions

Fig. 1. Schematic illustration of synthesis of the porous doped carbon nanostructures prepared using a template method.

Fig. 2. FE-SEM and FE-TEM images, and STEM-EDX elemental mapping images of (a,d, and g) PVP-C, (b,e, and h) Co-PVP-C, and (c,f, and i) Fe-PVP-C nanostructures. Scale bars: 200 nm.

Fig. 3. XPS N1s spectra of (a) PVP-C, (b) Co-PVP-C, and (c) Fe-PVP-C nanostructures. (d) Composition of N species of the as-prepared nanostructures.

Fig. 4. CVs of (a) PVP-C, (b) Co-PVP-C, and (c) Fe-PVP-C in Ar- or O₂-saturated 0.1 M NaOH with a scan rate of 50 mV s⁻¹ at room temperature. (d) ORR polarization curves of PVP-C, Co-PVP-C, Fe-PVP-C, and Pt/C electrocatalysts. (e) Koutecky-Levich plots of as-prepared samples at 0.7 V. (f) Comparison of onset potential and half-wave potential of PVP-C, Co-PVP-C, Fe-PVP-C and Pt/C electrocatalyst.

Fig. 5. Polarization curves of (a) PVP-C, (b) Co-PVP-C, (c) Fe-PVP-C, and (d) Pt/C with a scan rate of 5 mV s⁻¹ and an electrode rotation rate of 1600 rpm in O₂-saturated 0.1 M NaOH solution with and without 0.5 M CH₃OH.

Figure 1. S. Lee and Y.-W. Lee *et al.*

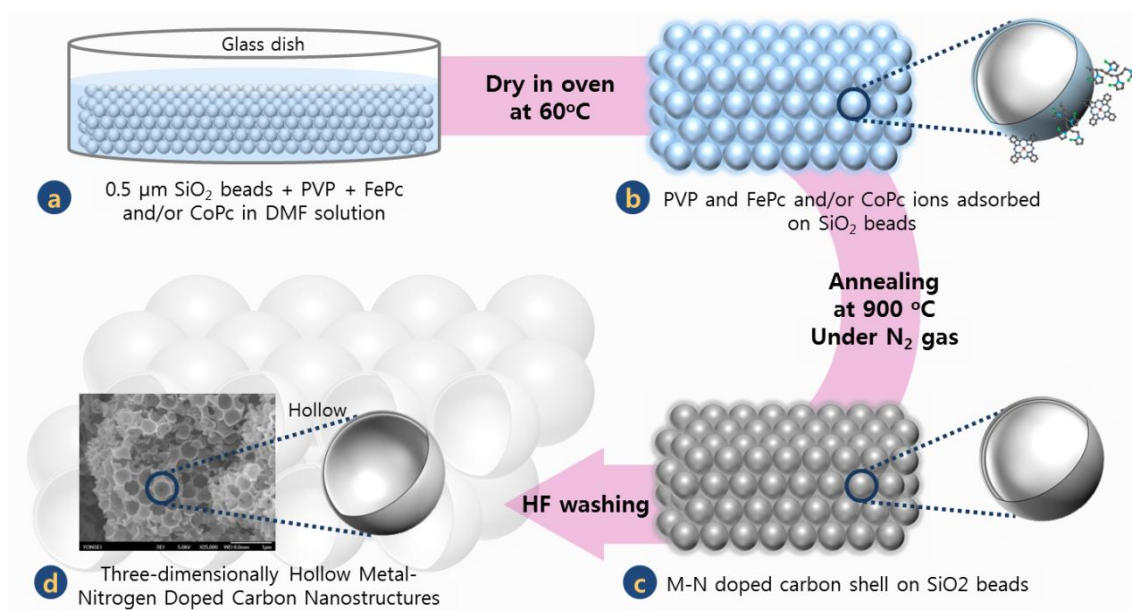


Figure 2. S. Lee and Y.-W. Lee *et al.*

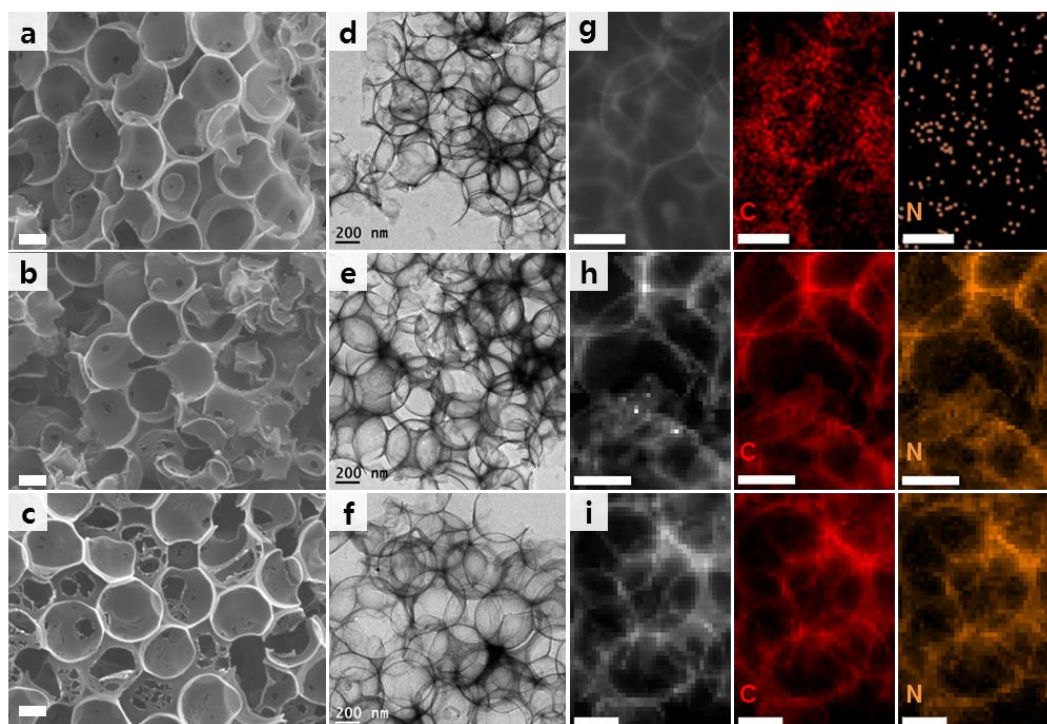


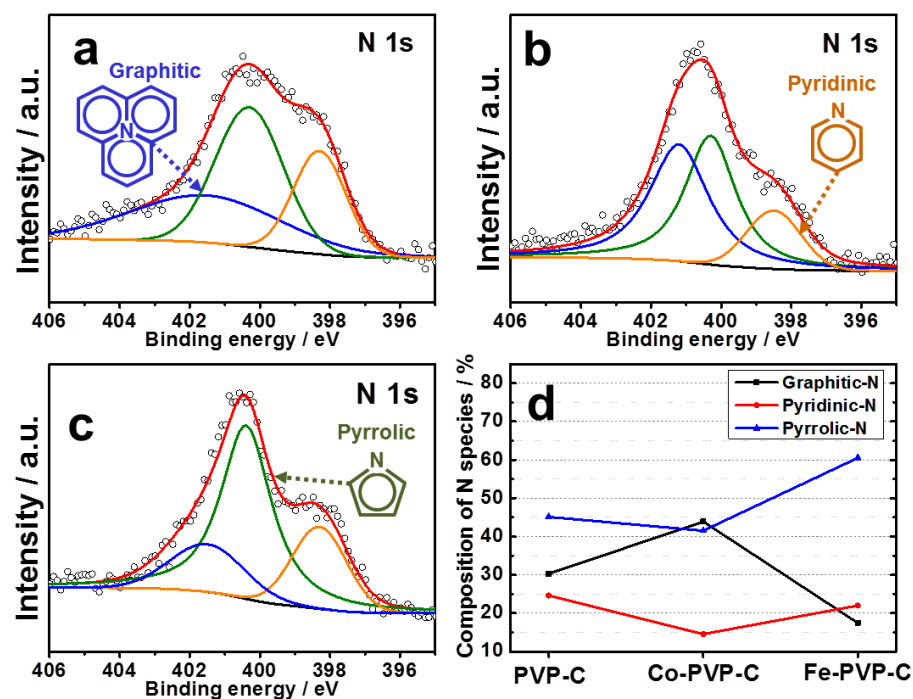
Figure 3. S. Lee and Y.-W. Lee *et al.*

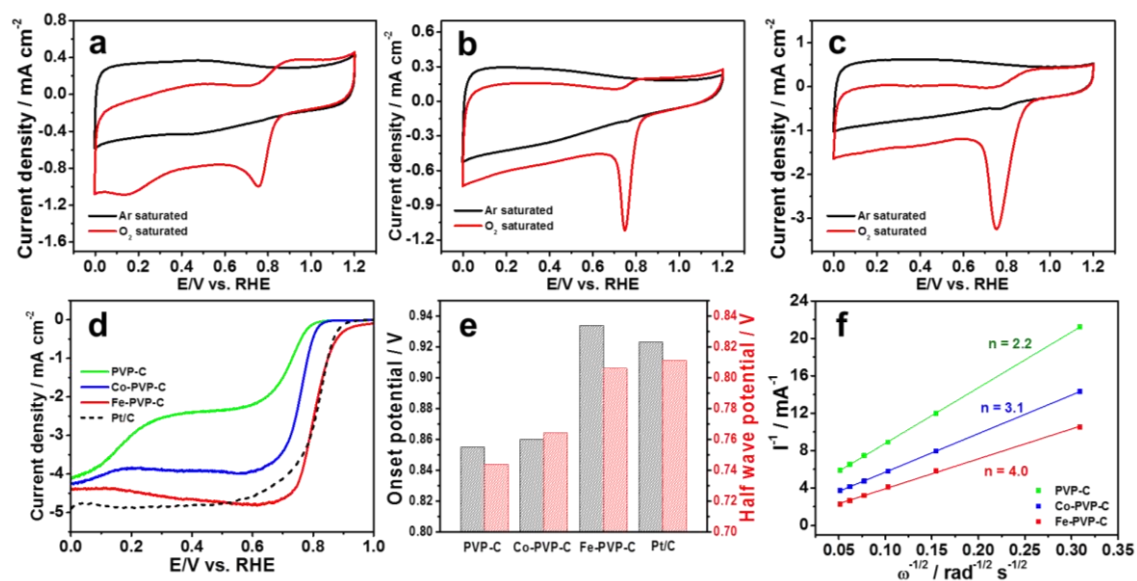
Figure 4. S. Lee and Y.-W. Lee *et al.*

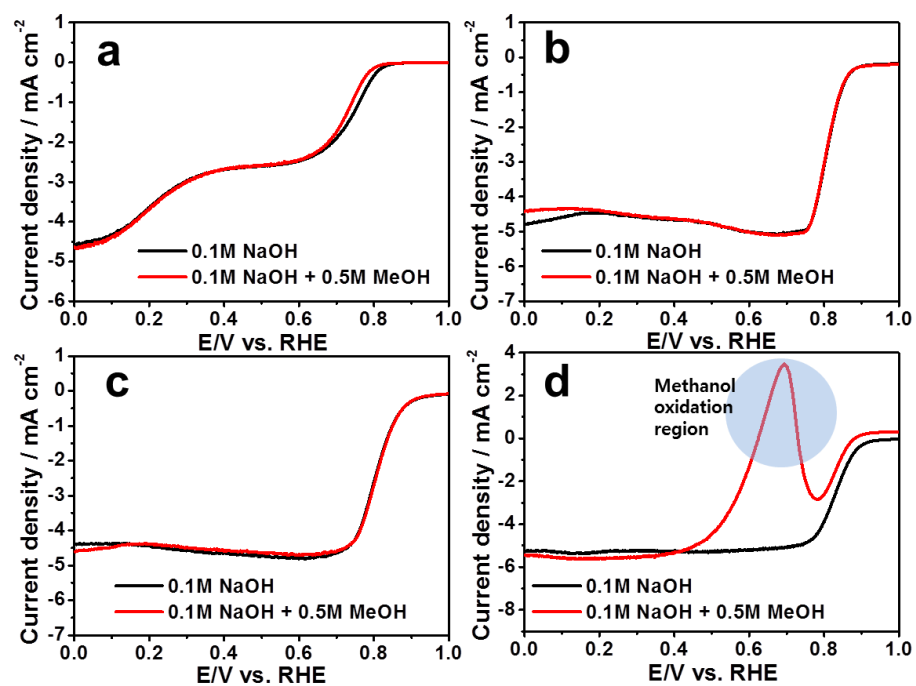
Figure 5. S. Lee and Y.-W. Lee *et al.*

Table 1. Elemental contents of the as-prepared nanostructures measured by XPS analysis

	C	O	N	Fe	Co
Fe-PVP-C	93.18 at%	4.55 at%	1.90 at%	0.37 at%	-
Co-PVP-C	92.69 at%	5.56 at%	1.52 at%	-	0.22 at%
PVP-C	93.45 at%	5.51 at%	1.03 at%	-	-

Supporting Information

Three-Dimensional Porous Metal-Nitrogen Doped Carbon Nanostructure as a Superior Non-Precious Electrocatalyst in Oxygen Reduction Reaction

Seul Lee,^{a,1} Young-Woo Lee,^{a,b,1} Da-Hee Kwak,^a Jin-Yeon Lee,^a Sang-Beom Han,^a

Jung Inn Sohn,^b Kyung-Won Park^{a,*}

^a Department of Chemical Engineering, Soongsil University, Seoul 156-743, Republic of Korea.

^b Department of Engineering Science, University of Oxford, Oxford OX1 3PJ, United Kingdom.

¹ These authors contributed equally to this work.

* Corresponding author. Tel: 82-2-820-0613. Fax: 82-2-812-5378.

E-mail address: kwpark@ssu.ac.kr (Prof. K.-W. Park).

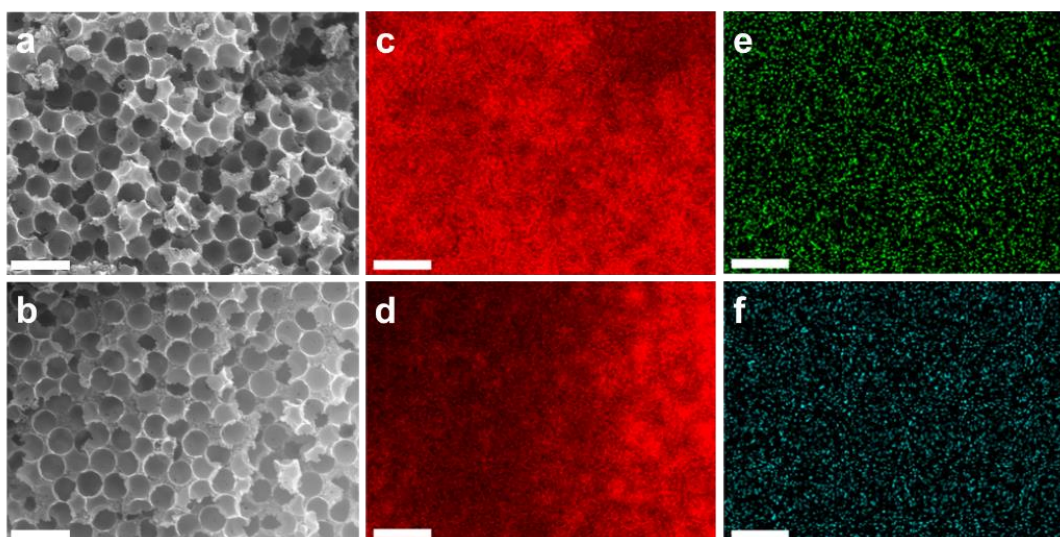


Fig. S1. FE-SEM images of (a) Fe-PVP-C and (b) Co-PVP-C nanostructures. EDX element mapping images of the Fe-PVP-C nanostructures for the carbon (c, red) and iron (e, green). EDX element mapping images of the Co-PVP-C nanostructures for the carbon (d, red) and cobalt (f, blue). Scale bars: 1 μm .

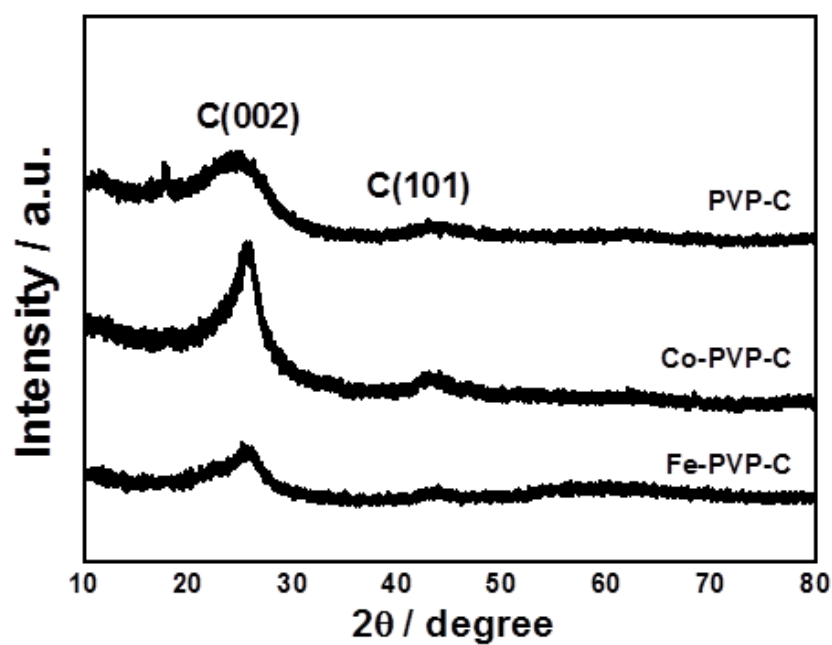


Fig. S2. XRD patterns of the PVP-C, Co-PVP-C, and Fe-PVP-C.

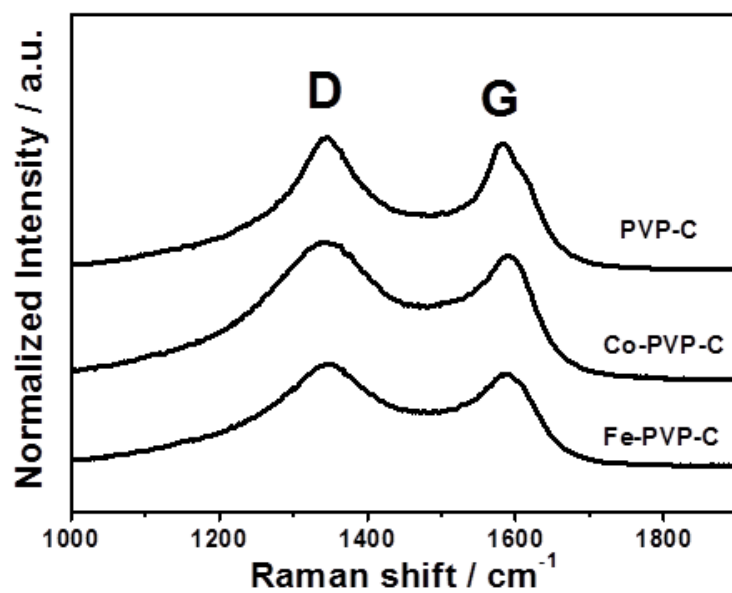


Fig. S3. Raman spectra of the PVP-C, Co-PVP-C, and Fe-PVP-C.

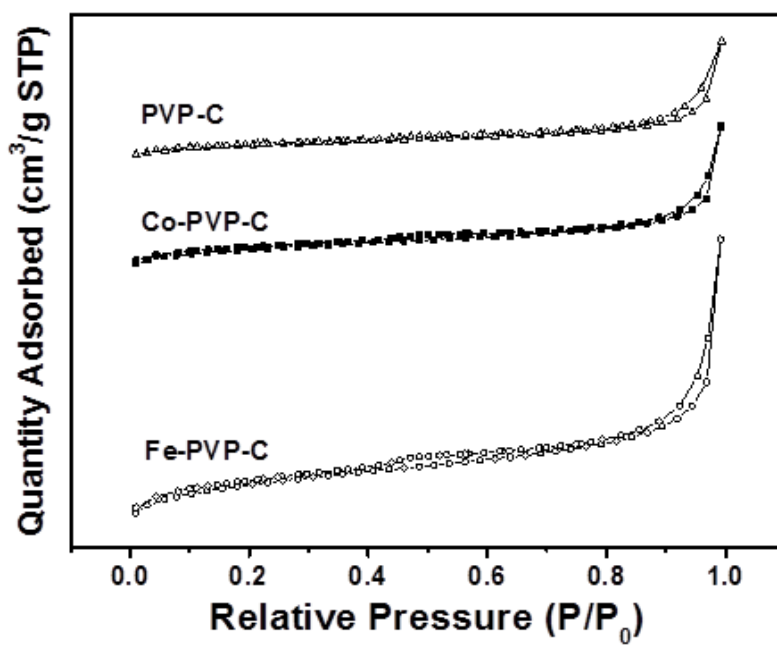


Fig. S4. Nitrogen adsorption/desorption isotherms of the PVP-C, Co-PVP-C, and Fe-PVP-C.

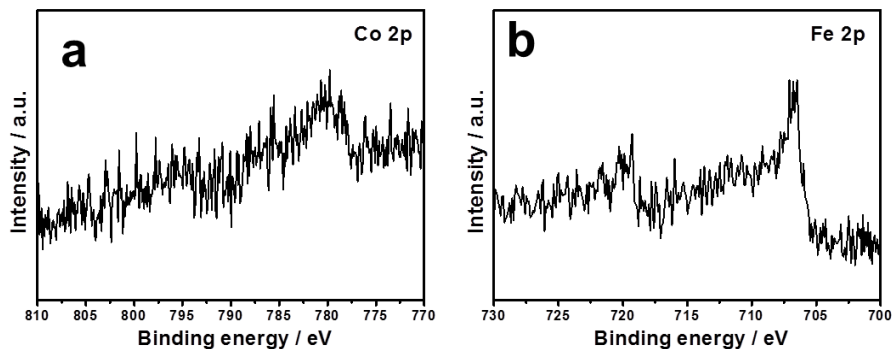


Fig. S5. (a) Co 2p XPS spectrum of the Co-PVP-C. (b) Fe 2p XPS spectrum of the Fe-PVP-C.

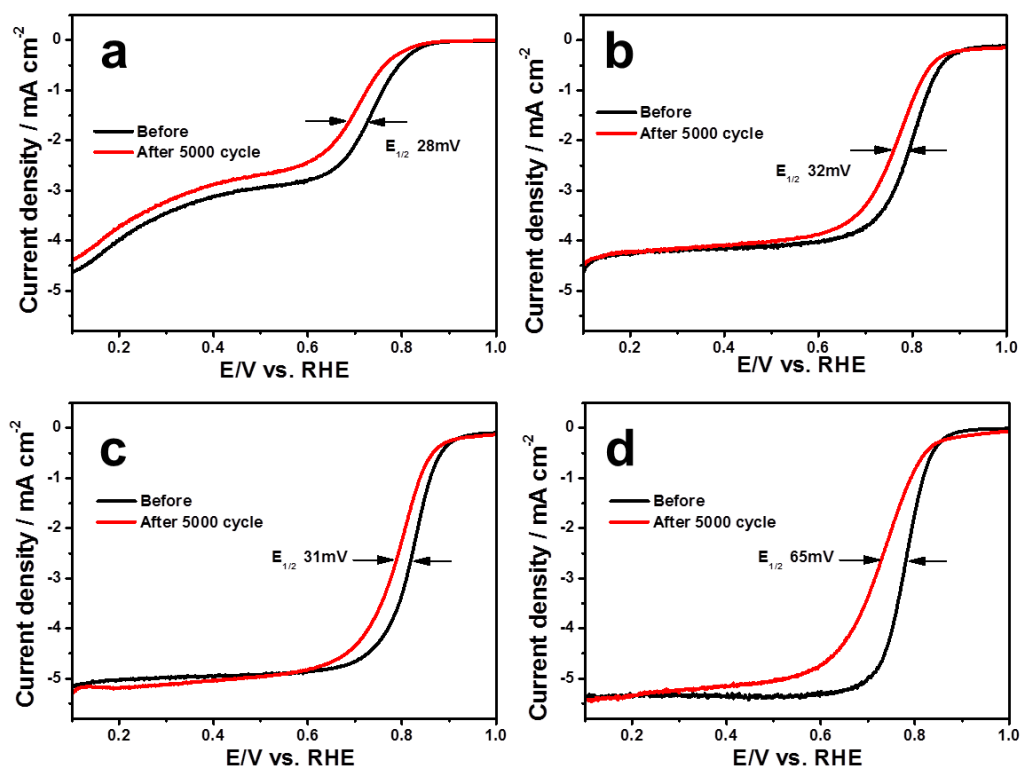


Fig. S6. ORR Polarization curves of (a) PVP-C, (b) Co-PVP-C, (c) Fe-PVP-C and (d) Pt/C before and after stability in O₂-saturated 0.1 M NaOH solution with a scan rate of 5 mV s⁻¹ and an electrode rotation rate of 1600 rpm at room temperature.

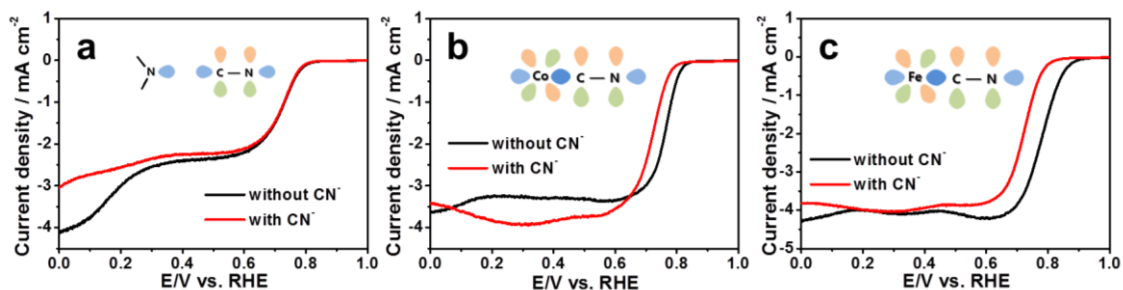


Fig. S7. Polarization curves of (a) PVP-C, (b) Co-PVP-C, and (c) Fe-PVP-C with a scan rate of 5 mV s⁻¹ and an electrode rotation rate of 1600 rpm in O₂-saturated 0.1 M NaOH solution w/ and w/o 10 mM KCN.

Table S1. Comparison of electrocatalytic properties of the previously reported non-precious electrocatalysts for ORR

Catalysts	Electrolyte	Reference electrode	Half wave potential	Electron transfer number (n)	
Fe-PVP-C	0.1 M NaOH	vs. RHE	0.81 V	~3.99	This work
Fe-N/C	0.1 M KOH	vs. RHE	0.80 V	~3.9	R S1
Iron carbide/N-doped carbon composite	0.1M NaOH	vs. RHE	0.72 V	~3.85	R S2
Cobalt doped nanoporous hollow carbon spheres	0.1 M KOH	vs. RHE	0.65 V	~3.8	R S3
Nitrogen-doped porous carbons	0.1 M KOH	vs. RHE	0.70 V	~3.89	R S4
Nitrogen-doped carbon sheets	0.1 M KOH	vs. RHE	0.71 V	~3.85	R S5
Iron nitride and nitrogen-doped graphene	0.1 M KOH	vs. Ag/AgCl	-0.18 V (0.72 vs. RHE)	~4	R S6
Heteroatom nitrogen-carbon nanosphere	0.1 M KOH	vs. Ag/AgCl	-0.12 V (0.78 vs. RHE)	~3.98	R S7
Nitrogen doped winged carbon nanotubes	0.1 M KOH	vs. RHE	0.79 V	~4	R S8
Bamboo-like carbon nanotube/Fe ₃ C nanoparticle	0.1 M KOH	vs. RHE	0.83 V	~3.99	R S9
Cheap carbon black based Fe-N _x /C	0.1 M KOH	vs. RHE	0.87 V	~3.9	R S10

Supporting References

- [R S1] L. Lin, Q. Zhu, A.-W. Xu, J. Am. Chem. Soc. 136 (2014) 11027-11033.
- [R S2] L. Gu, L. Jiang, J. Jin, J. Liu, G. Sun, Carbon 82 (2015) 572-578.
- [R S3] H. Wang, X. Bo, A. Wang, L. Guo, Electrochem. Commun. 36 (2013) 75-79.
- [R S4] Zhang, F. Sun, Z. Xiang, Z. Shen, J. Yun, D. Cao, Energy Environ. Sci. 7 (2014) 442-450.
- [R S5] G. Nam, J. Park, S. T. Kim, D. Shin, N. Park, Y. Kim, J.-S. Lee, J. Cho, Nano Lett. 14 (2014) 1870-1876.
- [R S6] H. Yin, C. Zhang, F. Liu, Y. Hou, Adv. Funct. Mater. 24 (2014) 2930-2937
- [R S7] D. Kim, O. L. Li, N. Saito, Phys. Chem. Chem. Phys. 16 (2014) 14905-14911.
- [R S8] Y. Cheng, H. Zhang, C. V. Varanasi, J. Liu, Sci. Rep. 3 (2013) 3195.
- [R S9] W, Yang, X. Liu, X. Yue, J. Jia, S. Guo, J. Am. Chem. Soc. 137 (2015) 1436-1439.
- [R S10] P. Song, Y. Zhang, J. Pan, L. Zhuang, W. Xu, Chem. Commun. 51 (2015) 1972-1975.